Available online at www.sciencedirect.com
ScienceDirect
Trans. Nonferrous Met. Soc. China 32(2022) 3321−3333
Transactions of Nonferrous Metals Society of China
www.tnmsc.cn

# One-step electrodeposition to fabricate robust superhydrophobic silver/graphene coatings with excellent stability

De-xin CHEN[1,2], Ye-qing HE[3], Qi-wei WANG[1], Wei LI[1], Zhi-xin KANG[3]

1. Institute of Advanced Wear & Corrosion Resistant and Functional Materials, Jinan University, Guangzhou 510632, China;
2. Shaoguan Research Institute of Jinan University, Shaoguan 512027, China;
3. School of Mechanical & Automotive Engineering, South China University of Technology, Guangzhou 510640, China

Received 24 August 2021; accepted 6 April 2022

**Abstract:** A facile method was proposed to prepare stretchable silver-based composite coatings with excellent conductivity and stability for flexible electronics. Silver coating was firstly deposited on thermoplastic polyurethane (TPU) elastomer rubber surface via two-component spraying technique, then the superhydrophobic surface was obtained by one-step electrodeposition of cerium compounds (CeM) and graphene nanosheets (GNS) to produce Ag/CeM/GNS composite coatings. The obtained Ag/CeM/GNS composite coatings maintained high conductivity after experiencing bending cycles and stretching cycles. Furthermore, the as-prepared Ag/CeM/GNS composite coatings showed excellent self-cleaning and anti-fouling properties, and the corrosion resistance has improved significantly compared to the original Ag coating. In addition, the Ag/CeM/GNS composite coatings could drive the circuit normally in the states of tensile, bending and twisting deformation, showing excellent mechanical stability and applicability. As a result, it is believed that the prepared Ag/CeM/GNS composite coatings with excellent conductivity and stability have promising applications for flexible electronics in harsh conditions.
**Key words:** silver/graphene coating; superhydrophobicity; one-step electrodeposition; stability

## 1 Introduction

In comparison to traditional rigid electronic devices, flexible electronic devices can meet the needs of various occasions thanks to their flexibility and malleability [1−3]. Recent advances and the diversity of materials used as electrodes have been developed for various flexible electronic applications [4−7]. Flexible electronic technology has been applied in electronic information, biomedicine, energy industry and national defense, such as wearable electronic devices [8], medical monitors [9], flexible displays [10] and flexible solar panels [11]. Flexible circuit board is the basic technology of flexible electronic, whose key technology involved is surface metallization. However, conductive metal coatings still face corrosion problems, resulting in a deterioration of the reliability and stability of flexible electronic devices [12−14].

Fabricating superhydrophobic coating on the surface of metallic conductive coating can effectively slow down the corrosion rate and improve the corrosion resistance of the coating [15−17]. If the superhydrophobic coating is too thick, the overall resistivity of the coating will increase and the conductivity will decrease, which will affect the practical application of the coating. For flexible electronic materials, it is very

**Corresponding author:** Qi-wei WANG, Tel: +86-20-85220890, E-mail: wangqiwei@jnu.edu.cn;
Zhi-xin KANG, Tel: +86-20-87111116, E-mail: zxkang@scut.edu.cn
DOI: 10.1016/S1003-6326(22)66023-0

important to maintain excellent conductivity. So, it is feasible to introduce materials with excellent conductivity as mixed phase for composite coatings [18,19].

Graphene is a two-dimensional carbon material, which has stable physical and chemical properties and excellent conductivity, and it is an ideal material for the preparation of conductive composite coatings [20,21]. ZHOU et al [22] prepared uniform and dense Ag/graphene nanosheet (Ag/GNS) composite films on the modified polyethylene terephthalate (PET) substrates via a novel method of three-component spray-spin-spray coating, and the sheet resistance of Ag/GNS-5 composite films was reduced by 60% compared to the pristine Ag films. WU et al [23] developed ultra-light, high-performance electromagnetic interference shielding graphene foam/poly(3,4-ethylenedioxythiophene): poly(styrenesulfonate) composites by drop-coating of PEDOT: PSS on cellular-structured, freestanding GFs. The electrical conductivity was improved to be as high as 43.2 S/cm and the electromagnetic interference shielding effectiveness of composites could reach a remarkable value of 91.9 dB. However, these composites are lack of reliability for the practical application, which would need high stability, conductivity and anti-corrosion properties.

In this work, we presented a facile method to prepare stretchable silver-based composite coatings with excellent stability. Silver coating was firstly prepared on TPU surface of elastic substrate via two-component spraying method, then the super-hydrophobic surface was obtained by one-step electrodeposition of cerium nitrate hexahydrate and tetradecanoic acid. During electrodeposition, GNS was added to the electrodeposition solution, and Ag/CeM/GNS (CeM represents cerium compounds) composite coatings were obtained. The electronic conductivity, mechanical stability, and corrosion resistance of these composite coatings were studied to explore the practical application possibility for flexible electronic.

## 2 Experimental

### 2.1 Materials

TPU elastomer rubber with a thickness of 0.8 mm was provided by Shenzhen Guofeilong Trade Co., Ltd. Graphene nanosheets with particle diameters of 5−10 μm were purchased from Aladdin Biochemical Technology Co., Ltd. Stannous chloride ($SnCl_2·2H_2O$, 98%), hydrochloric acid (HCl, 37%) and ammonium hydroxide ($NH_3·H_2O$, 25%) were all obtained from Guangzhou Chemical Reagent Factory. Silver nitrate ($AgNO_3$, 99.8%), glyoxal ($(CHO)_2$, 30%) and triethanolamine ($N(CH_2CH_2OH)_3$, 85%) were purchased from Sinopharm Chemical Reagent Co., Ltd. Cerium (III) nitrate hexahydrate ($Ce(NO_3)_3·6H_2O$, 98%) and myristic acid ($C_{14}H_{28}O_2$, 99.5%) were supplied by Aladdin Industrial Corporation. All reagents were used as received without further purification.

### 2.2 Pretreatment of TPU substrate

The pretreatment process of the TPU substrate included alkali washing, P-TES grafting, N-TES grafting and sensitization, as shown in Fig. 1. TPU substrate was put in an 80 °C alkali washing solution (80 g/L NaOH and 15 g/L $Na_2CO_3$) for 30 min to remove the stains on the surface of the substrate. After alkali washing, the species was immersed in P-TES alcohol solution (0.8 g/L P-TES) at room temperature for 30 s, and then irradiated with an ultraviolet lamp (365 nm and 2.4 J/cm$^2$) for 5 min to complete the photo grafting of P-TES molecules on TPU surface. After that, the sample was immersed in N-TES aqueous solution (1 g/L N-TES) at room temperature for 10 min to graft N-TES molecules onto the surface of the sample. The grafted TPU substrate was immersed in $SnCl_2$ aqueous solution (0.09 mol/L $SnCl_2$ and 1.30 mol/L HCl) at room temperature for 20 min, and then washed with deionized water and dried, waiting for electroless spraying.

### 2.3 Preparation of Ag coating on TPU surface

After surface pretreatment, the TPU sample was fixed in the glovebox, and the distance between the nozzle and the sample surface was kept at 10 cm. Silver ammonia solution (0.1 mol/L silver nitrate and 0.2 mol/L ammonium hydroxide) and reducing agent (0.3 mol/L glyoxal ($C_2H_2O_2$) and 0.1 mol/L triethanolamine $N(HOCH_2CH_2)_3$) were evenly sprayed onto the TPU sample surface. After spraying, a large amount of deionized water was used to remove the residual solvent on the surface of the sample, and the sample was dried in a vacuum drying oven at 60 °C for 12 h.

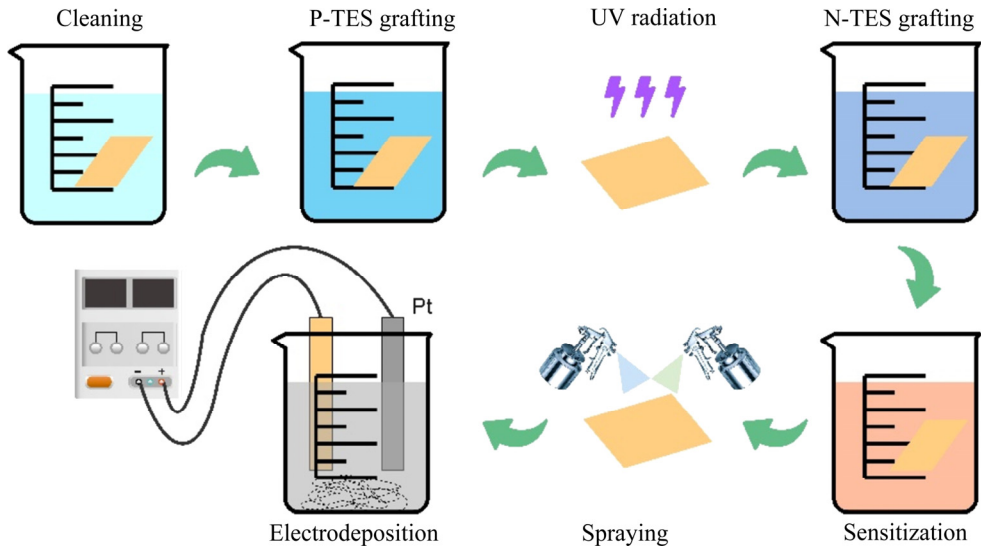


**Fig. 1** Schematic illustration of fabrication procedures of Ag/CeM/GNS composite coatings

### 2.4 Preparation of superhydrophobic coating by electrodeposition

Cerium nitrate hexahydrate ($Ce(NO_3)_3·6H_2O$) and tetradecanoic acid ($C_{14}H_{28}O_2$) were added into anhydrous ethanol, and then 0, 1, 3 and 5 g/L graphene nanosheets were added into anhydrous ethanol, respectively. Full stirring and ultrasonic vibration were carried out until the graphene nanosheets were evenly dispersed in anhydrous ethanol. The concentrations of cerium nitrate hexahydrate and tetradecanoic acid were 0.05 mol/L and 0.1 mol/L, respectively. Superhydrophobic coatings were prepared through electrodeposition using a direct current power supply (Zhaoxin RXN−605D) at room temperature. The platinum plate was used as the anode while the sample after spraying silver was used as the cathode, the distance between the anode and cathode was controlled at 2 cm, the deposition voltage was 20 V, and the deposition time was 20 min. After electrodeposition, the samples were taken out from the electrolyte, washed several times with anhydrous ethanol, and then dried in a vacuum oven at 60 °C for 12 h. The samples were numbered as Ag/CeM, Ag/CeM/GNS-1, Ag/CeM/GNS-3, and Ag/CeM/GNS-5, respectively.

### 2.5 Characterization

The contact angle (CA) of the sample surface was measured by a contact angle measuring instrument (OCA35, DataPhysics, Germany). The droplet used in the test was distilled water, and its volume of the droplet was 5 μL. Five points were tested for each sample, and the average value of the results was taken. The surface morphology and graphene distribution of the composite coating were observed by field emission scanning electron microscope (Zeiss Merlin, Carl Zeiss AG, Germany), and the element content of the composite coating was analyzed by EDS electron probe analysis system (X-Maxn20 double-detector system). The surface profiler (UP Dual Model) was used to observe the surface profile of the sample, and the surface roughness of the sample was calculated by guiding software. X-ray diffraction (D8 advance, Bruker, Germany) was used to analyze the phase of the composite coating and the scanning range was 5°−90°.

In addition, the resistivity of the coating was tested by four-probe resistance measuring instrument (RTS−8, Guangzhou Four-probe Technology Co., Ltd.). Five positions were measured for each sample, and the average value was taken as the resistivity of the sample, so as to ensure the accuracy and reliability of the experimental data. Potentiodynamic polarization curve and electrochemical impedance spectroscopy (EIS) were used to evaluate the corrosion resistance of the composite coating by electrochemical work station (CHI760E, Shanghai Chenhua Instrument Co., Ltd.). The test area of the sample was 1 $cm^2$. The three-electrode system was used in the test, i.e., the composite coating was used as the working electrode, the platinum electrode was used as the counter electrode, and the KCl-saturated Ag/AgCl electrode was used as the reference electrode. The

electrolyte solutions used in the test were 3.5 wt.% NaCl solution. Among them, the test range of potentiodynamic polarization curve is from −1000 to 1000 mV versus open circuit potential (OCP) with a scanning rate of 10 mV/s, and the test frequency range of electrochemical impedance spectrum was 10 mHz−100 kHz.

## 3 Results and discussion

### 3.1 Composition and surface morphology of Ag/CeM/GNS composite coatings

Figure 2 shows the surface micromorphology of the TPU substrate and Ag/CeM/GNS composite coatings. It could be observed that the surface of TPU substrate was flat and smooth (Fig. 2(a)). After increasing the magnification of SEM, it could be observed that there are many nanoscale pores evenly distributed over the surfaces (Fig. 2(e)). After two-component spraying, the surface of TPU was covered with silver nanoparticles to form a dense silver layer, as shown in Figs. 2(b) and (f). After electrodeposition, the coral-like, rough and porous structure was formed, and the graphene was embedded in the rough structure evenly (Figs. 2(c, g)). As the graphene content of an electrolytic solution increased, the graphene content of composite coatings increased as well. When the concentration of graphene in the electrolyte solution was 5 g/L, the surface of the sample was basically covered by graphene, and the flakes of graphene deposited on the sample surface crisscrossed and stacked with each other, forming a new micro-nano rough structure, as shown in Figs. 2(d) and (h).

Figures 2(i−n) show the element surface scanning of Ag/CeM/GNS-3 composite coating, demonstrating the chemical composition of the composite coating. It was clear that Ce, Ag, O and C elements were evenly distributed on the surface of the sample, indicating that the silver nanoparticles, cerium tetradecanoate and graphene in the composite coating were evenly distributed without obvious regionality.

XRD is a common method to analyze the chemical composition of materials. The XRD patterns of TPU substrate and Ag/CeM/GNS composite coatings are illustrated in Fig. 3(a). Compared with the original TPU substrate, a group

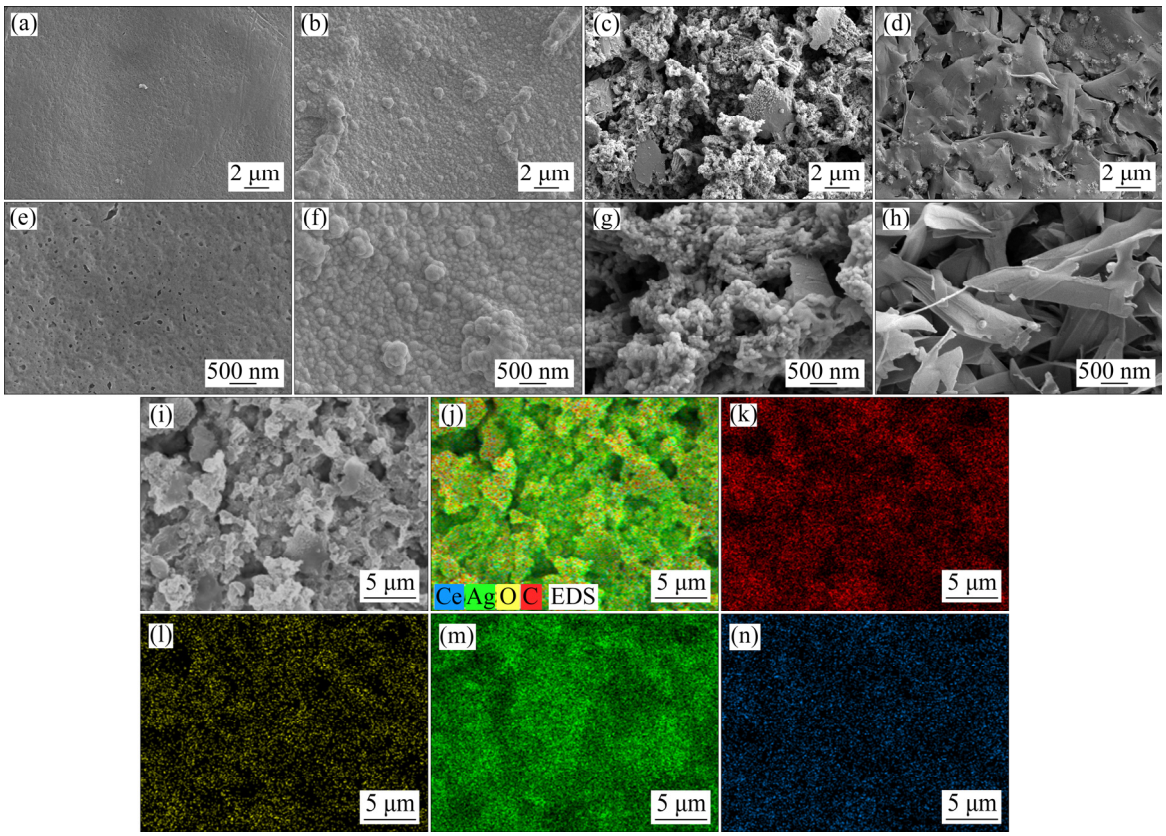


**Fig. 2** SEM images of samples: (a, e) TPU substrate; (b, f) Ag coating; (c, g) Ag/CeM/GNS-3 composite coating; (d, h) Ag/CeM/GNS-5 composite coating; (i) SEM image for EDS; (j−n) Elemental mapping of Ag/CeM/GNS-3 composite coating

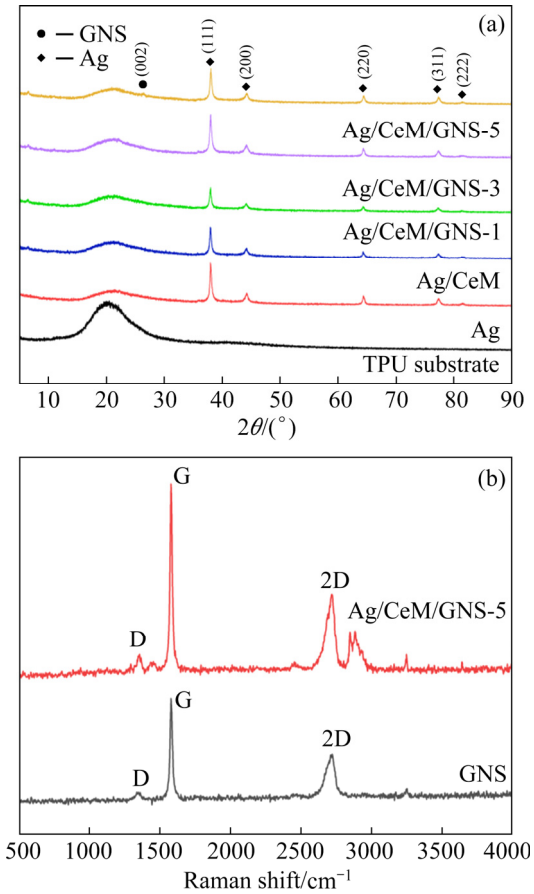


**Fig. 3** XRD patterns of TPU substrate, Ag, Ag/CeM, Ag/CeM/GNS-1, Ag/CeM/GNS-3, and Ag/CeM/GNS-5 composite coatings (a), and Raman spectra of GNS and Ag/CeM/GNS-5 composite coating (b)

of new diffraction peaks appeared at $2\theta$ values of 38.1°, 44.3°, 64.4°, 77.4° and 81.5° for the samples after silver spraying, which corresponded to (111), (200), (220), (311) and (222) crystal planes of silver, respectively [24]. In addition, no peak of silver oxide was found in the XRD pattern, indicating that the silver coating was formed in the form of the simple substance on the surface of TPU. The XRD patterns of Ag/CeM/GNS-1, Ag/CeM/GNS-3 and Ag/CeM/GNS-5 samples were observed. It was found that a new diffraction peak appeared at $2\theta$=26°, which corresponded to the (002) crystal plane of grapheme [25]. It was proved that the graphene in electrolyte solution was deposited on the sample surface with cerium tetradecanoate after electrodeposition.

In order to further confirm the existence of graphene in the composite coatings, Raman spectrum was used to analyze the composite coatings. As shown in Fig. 3(b), the obvious characteristic peaks at 1349.1, 1584.4 and 2720.9 $cm^{-1}$, namely D, G and 2D peaks of grapheme, respectively, can be observed [26]. The Raman spectra of Ag/CeM/GNS-5 composite coating also showed the above characteristic peaks, and the graphene in Ag/CeM/GNS-5 composite coating was further confirmed.

### 3.2 Surface wettability and self-cleaning performance of Ag/CeM/GNS composite coatings

Figure 4(a) shows the contact angles (CA) of distilled water on the surface of Ag/CeM/GNS composite coatings. It can be seen from Fig. 4(a) that the contact angle of Ag coating was 75.3° before electrodeposition, showing the hydrophilic surface. After electrodeposition, the contact angles of Ag/CeM, Ag/CeM/GNS-1, Ag/CeM/GNS-3 and Ag/CeM/GNS-5 were 152.5°, 152.8°, 153.7° and 154.1°, respectively, which were more than 150°. It was worth noting that the contact angles of the

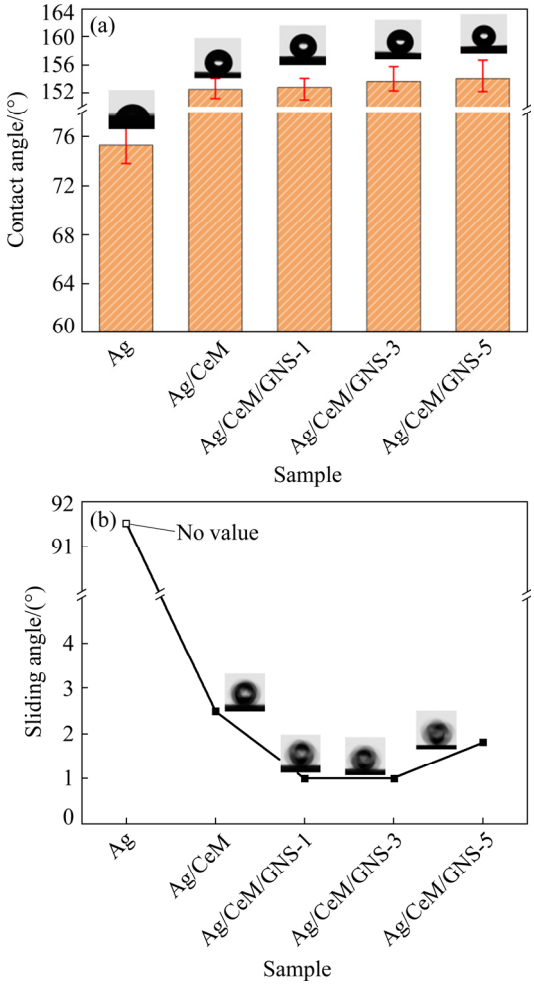


**Fig. 4** Contact angle (a) and sliding angle (b) of distilled water on surface of composite coatings

composite coatings increased slightly with the increase of grapheme content. The above results showed that the electrodeposited samples could obtain superhydrophobic effect whether the electrolyte solution contained graphene or not. The key to obtain superhydrophobic properties of the samples was the deposition of cerium tetradecanoate with low surface energy and the construction of micro-nano structure. After the introduction of graphene, the contact angles of the composite coatings increased in a certain range, indicating that the deposition of graphene promoted the construction of superhydrophobic surface.

Sliding angle (SA) is also an important parameter to reflect superhydrophobic properties. As shown in Fig. 4(b), the sliding angle of the Ag coating cannot be measured due to good hydrophilicity, and the water droplets on the surface of the sample will not fall off even after 180° upside down. The sliding angles of Ag/CeM, Ag/CeM/GNS-1, Ag/CeM/GNS-3 and Ag/CeM/GNS-5 were 2.5°, 1°, 1° and 1.8°, respectively, and less than 5°, indicating that the electrodeposited samples obtained excellent superhydrophobic properties.

The 3D profile of the sample surface could be obtained by optical scanning of the composite coatings. Figure 5 shows the 3D contour image of each sample surface. It could be observed from Fig. 5 that the surface of the Ag coating was relatively flat with some protrusions. After electrodeposition, a large number of micron scale mountain-like protrusions appeared on the surface of the Ag/CeM sample, and these protrusions were different in height, forming a rough surface. When 1 g/L GNS was added into the electrolyte solution, the protrusions on the surface of the sample became smaller, but the number of protrusions increased. When the GNS content in the electrolyte solution increased to 3 g/L, the protrusions on the surface of the sample began to coarsen again, and the shape was no longer as sharp as that of Ag/CeM/GNS-1. When the GNS content continued to increase to 5 g/L, the protrusions on the surface of the sample showed obvious difference, some protrusions continued to coarsen, and some still kept the shape of spines. In order to further analyze the 3D profile of each sample surface, the surface roughness ($R_a$) value of the sample was calculated by Gwyddion software, and the results are shown in Table 1. The results showed that the $R_a$ values of Ag, Ag/CeM, Ag/CeM/GNS-1, Ag/CeM/GNS-3 and Ag/CeM/GNS-5 were 0.972, 2.046, 2.322, 2.339 and 2.634 μm, respectively. Compared to the pure Ag coating, the surface roughness of the electrodeposited samples increased greatly, and the $R_a$ value of Ag/CeM is over twice that of the silver coating. However, the $R_a$ value of the samples increased only slightly when GNS was added to the electrolyte solution. These results confirmed that the key to the formation of the superhydrophobic surface was the deposition of cerium tetradecanoate, but graphene would increase

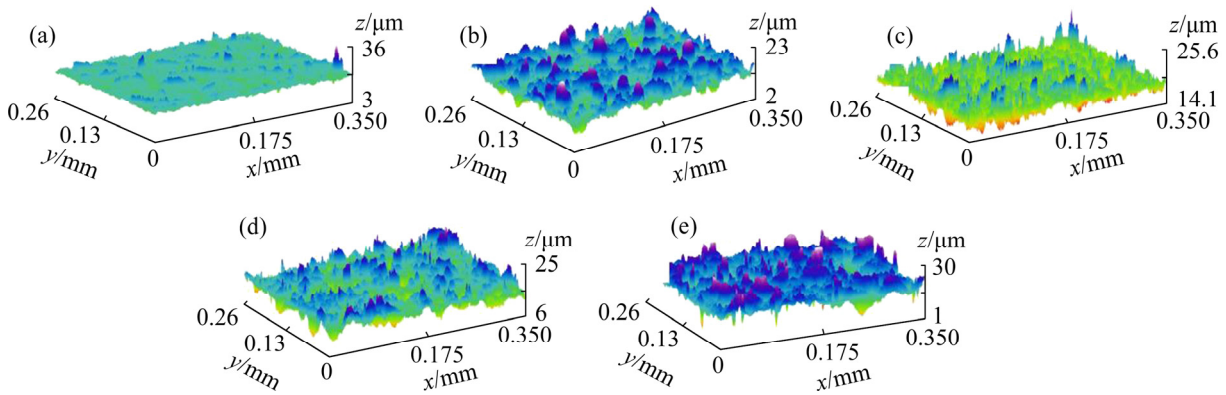


**Fig. 5** 3D profile images of composite coatings: (a) Ag; (b) Ag/CeM; (c) Ag/CeM/GNS-1; (d) Ag/CeM/GNS-3; (e) Ag/CeM/GNS-5

**Table 1** Surface roughness ($R_a$) values of composite coatings

| Coating | Ag | Ag/CeM | Ag/CeM/GNS-1 | Ag/CeM/GNS-3 | Ag/CeM/GNS-5 |
|---|---|---|---|---|---|
| $R_a$/μm | 0.972 | 2.046 | 2.322 | 2.339 | 2.634 |

the surface roughness and improve the super-hydrophobic properties.

Self-cleaning is an important performance of superhydrophobic materials. In order to verify the self-cleaning effect of the sample, 0.5 g of sediment was sprinkled on the surfaces of Ag coating and Ag/CeM/GNS-5 composite coating, respectively, and then water was dripped onto the sample surface with a rubber tipped dropper, as shown in Fig. 6. When water was dripped onto the surface of Ag coating, the water droplets adhered to the sample surface. After a period of time, a pool of water was formed on the sample surface, and there was no sign of rolling away, as shown in Figs. 6($a_1$−$a_4$). When water was dropped on the sample Ag/CeM/GNS-5, the water drops quickly rolled away from the sample surface and took away the sediment on the rolling path of the water drops, leaving an obvious track on the sample, as shown in Figs. 6($b_1$−$b_4$). After dropping water for a period of time, the sediment on the sample surface was taken away by the water drops, which perfectly showed its self-cleaning effect and formed a sharp contrast with the Ag coating surface.

Figures 6($c_1$−$c_3$) and ($d_1$−$d_3$) show the antifouling ability of the Ag coating and Ag/CeM/GNS-5 composite coating, respectively. The mud water mixture was made up by adding 20 g of soil into 200 mL of deionized water and stirring it evenly. The Ag coating and Ag/CeM/GNS-5 composite coatings were immersed in the mud water mixture for 5 s and taken out. It could be found that the mixed solution was adhered to the Ag coating and the surface of the Ag coating was polluted by the mixed solution, while the surface of Ag/CeM/GNS-5 was always dry and not polluted by the mixed solution. These results show that the Ag/CeM/GNS-5 coatings process an excellent antifouling effect and can be used in the harsh natural environment.

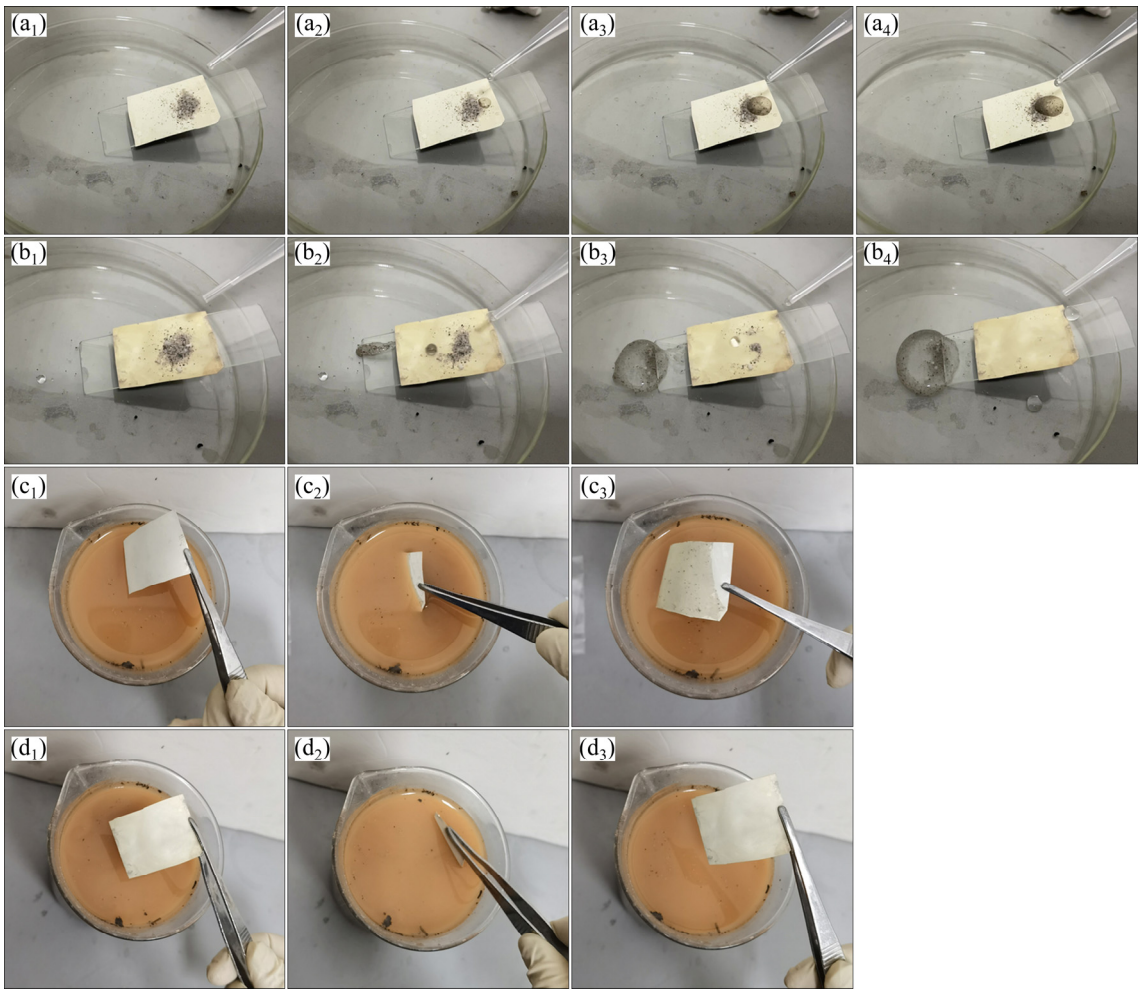


**Fig. 6** Self-cleaning experiment results ($a_1$−$a_4$, $b_1$−$b_4$) and anti-fouling experiment results ($c_1$−$c_3$, $d_1$−$d_3$): ($a_1$−$a_4$, $c_1$−$c_3$) Ag coating; ($b_1$−$b_4$, $d_1$−$d_3$) Ag/CeM/GNS-5 composite coating

### 3.3 Electrical properties and stability of Ag/CeM/GNS composite coatings

As a conductive coating material, electrical property is one of the most important properties. Figure 7(a) shows the resistivities of Ag/CeM/GNS composite coatings, and the resistivities of Ag, Ag/CeM/GNS-1, Ag/CeM/GNS-3 and Ag/CeM/GNS-5 coatings are 0.679, 1.667, 0.878, 0.535 and 0.494 Ω·mm, respectively. Because of the poor conductivity of cerium tetradecanoate, the cerium tetradecanoate covering on the silver layer after electrodeposition reduced the overall conductivity of the composite coating, so that the resistivity of Ag/CeM increased by 145.5% compared with that of the pure Ag coating. When GNS was added into the electrodeposition solution, GNS with good conductivity was deposited on the Ag coating with cerium tetradecanoate, which greatly improved the conductivity of the composite coating. Compared to Ag/CeM, the resistivities of Ag/CeM/GNS-1, Ag/CeM/GNS-3 and Ag/CeM/GNS-5 decreased by 47.3%, 68.3% and 70.7%, respectively, among which the resistivities of Ag/CeM/GNS-3 and Ag/CeM/GNS-5 were lower than that of the Ag coating without electrodeposition. Compared to the pure Ag coating, the resistivity of Ag/CeM/GNS-5 composite coating decreased by 27.2%, and the conductivity was greatly improved.

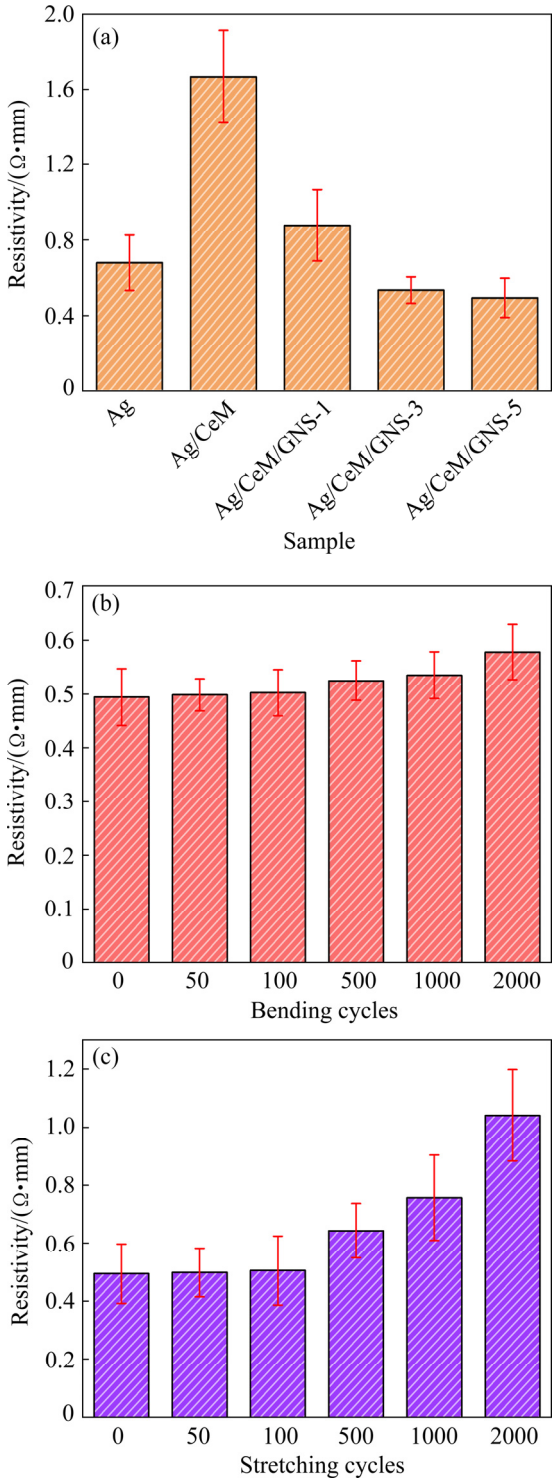


**Fig. 7** Resistivity of composite coatings (a), and variation of resistivity of Ag/CeM/GNS-5 composite coatings with bending cycles (b) and stretching cycles (c)

Figure 7(b) shows the change of resistivity of Ag/CeM/GNS-5 with different bending cycles. In the experiment, the sample was folded once along the central axis and unfolded, naming as a bending cycle. The original resistivity of Ag/CeM/GNS-5 was 0.494 Ω·mm. After experiencing 50, 100, 500, 1000 and 2000 bending cycles, the resistivity increased to 0.499, 0.502, 0.525, 0.535, 0.578 Ω·mm, respectively. In other words, the resistivity has increased by 1.0% (50 cycles), 1.6% (100 cycles), 6.3% (500 cycles), 8.3% (1000 cycles) and 17.0% (2000 cycles), respectively. When the bending cycles were less than 1000, there was no significant change of the resistivity of the Ag/CeM/GNS-5 composite coating, while the bending cycles were more than 1000, the resistivity increased slightly. These results showed that Ag/CeM/GNS-5 still maintained good conductivity after multiple bending, showing excellent bending resistance and conductivity stability.

As an elastic substrate, TPU material will inevitably be subjected to tensile stress when it is used in wearable electronics. When the substrate is stretched, elastic deformation will occur, and the conductive coating will also be deformed. Tiny cracks will appear on the surface of the coating, which will further reduce the electrical conductivity of the material and affect the practical application

of Ag/CeM/GNS composite coatings. Therefore, it is significant to study the relationship between the resistivity of Ag/CeM/GNS composite coatings and the number of tensile cycles, and the results are shown in Fig. 7(c). During the tensile test, one end of the sample was fixed with a collet, and the other end was applied with tensile stress until the length of the sample was 1.2 times of the original length ($\varepsilon$=20%). Then, the sample was slowly loosened, and the original length of the sample was restored. At this moment, a tensile cycle was completed. The original resistivity of Ag/CeM/GNS-5 was 0.494 Ω·mm. After experiencing 50, 100, 500, 1000 and 2000 tensile cycles, the resistivity of Ag/CeM/GNS-5 increased to 0.498, 0.505, 0.643, 0.757 and 1.041 Ω·mm, respectively. Compared with the original Ag/CeM/GNS-5, the resistivity increased by 0.8%, 2.2%, 30.2%, 53.2% and 110.7%, respectively. When tensile cycles were less than 100, the resistivity of Ag/CeM/GNS-5 was almost unchanged. When tensile cycles continued to increase, the resistivity increased significantly. When tensile cycles reached 2000, the resistivity became 2.1 times that of the original Ag/CeM/GNS-5. When only few tensile cycles were applied, the microcracks formed during the tensile process of the coating disappeared with the increase of the rebound of the substrate. With the increment of tensile cycles, the original microcracks will continue to expand and new microcracks will appear. When the substrate rebounds, the microcracks cannot be completely eliminated. The microcracks which are not eliminated are the key factors for the decrement of the conductivity of the composite coating.

In order to ensure that the Ag/CeM/GNs-5 composite coating can be applied to different occasions, the Ag/CeM/GNS-5 composite coating was connected into a simple circuit composed of DC power supply, light-emitting diode and wire (as shown in Fig. 8). Different stresses were applied to Ag/CeM/GNS-5 respectively to produce a variety of deformation. The original length of Ag/CeM/GNS-5 was 3 cm, and the diode was normally emitting at this time, as shown in Fig. 8(a). When the length of the sample was stretched to 4 cm, the diode could still work normally, and the brightness was not affected, as shown in Fig. 8(b). After that, whether the Ag/CeM/GNS-5 was bent or twisted, the circuit still conducted normally, and the

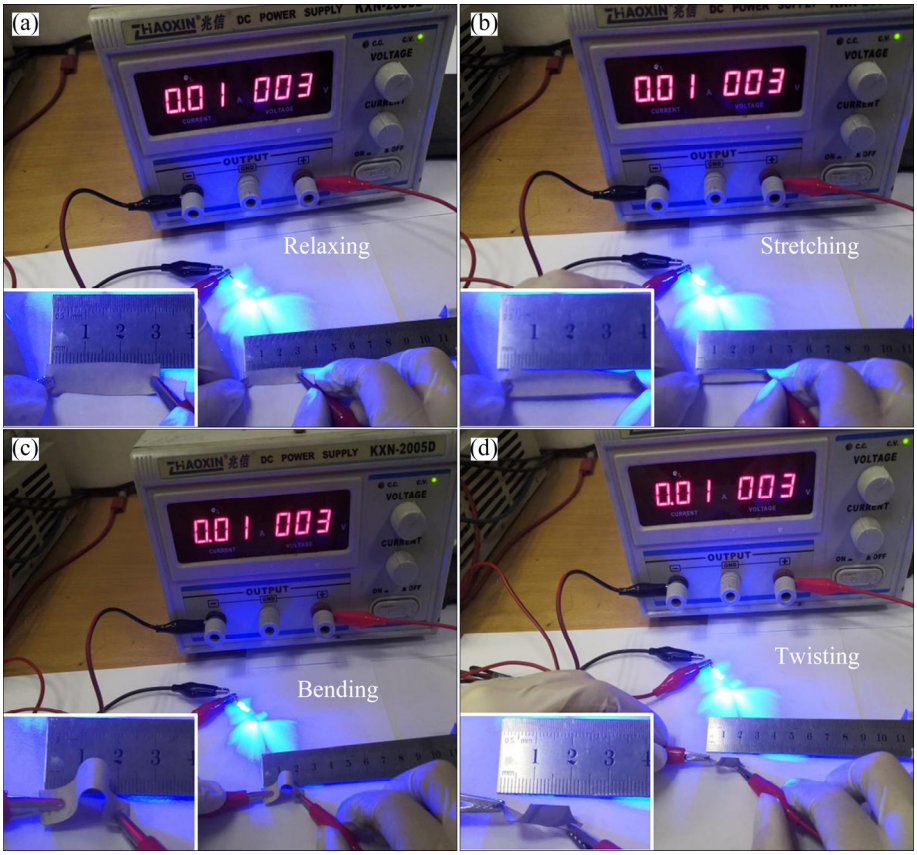


**Fig. 8** Electric circuits with Ag/CeM/GNS-5 composite coatings as conductor

brightness of the diode had no obvious change, as shown in Figs. 8(c, d). The above results showed that the Ag/CeM/GNS-5 composite coating on TPU substrate could be used as a good conductive material and could be applied to the complex stress environment.

### 3.4 Corrosion resistance of Ag/CeM/GNS composite coatings

The corrosion of flexible electronics is an important factor limiting its application. Therefore, it is an important way to broaden its application to study the corrosion performance and corrosion mechanism of flexible electronic materials so as to improve their corrosion resistance. In this section, the electrochemical corrosion behaviors of Ag/CeM/GNS composite coating in 3.5 wt.% NaCl solution and simulated sweat were studied, and the mechanism of improving its corrosion performance was analyzed.

Figure 9(a) shows potentiodynamic polarization curves of Ag and Ag/CeM/GNS-5 in 3.5 wt.% NaCl solution. Generally speaking, the smaller the corrosion current density in the potentiodynamic polarization curve, the lower the corrosion rate and the better the corrosion resistance of the material [27]. In order to quantitatively analyze the corrosion resistance of the samples, the corrosion current density ($J_{corr}$) and corrosion potential ($\varphi_{corr}$) in the polarization curve were obtained by the Tafel epitaxy method. The results are shown in Table 2. In NaCl solution, the corrosion current densities of Ag and Ag/CeM/GNS-5 are 6.209 and 0.388 μA/cm$^2$, respectively. After the super- hydrophobic surface was prepared, the corrosion current density of Ag/CeM/GNS-5 was obviously reduced, which was 1/16 that of the silver coating, and the corrosion resistance was significantly improved.

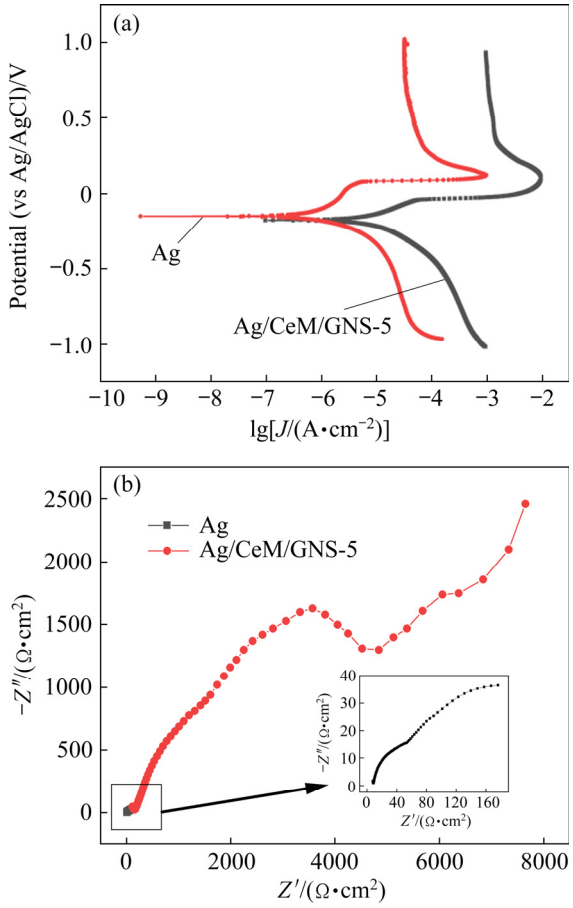


**Fig. 9** Polarization curves (a) and Nyquist curve (b) of Ag and Ag/CeM/GNS-5 composite coatings in 3.5 wt.% NaCl solution

**Table 2** Corrosion potential ($\varphi_{corr}$) and corrosion current density ($J_{corr}$) of Ag and Ag/CeM/GNS-5 composite coatings in 3.5 wt.% NaCl solution

| Coating | $\varphi_{corr}$ (vs Ag/AgCl)/V | $J_{corr}$/(μA·cm$^{-2}$) |
|---|---|---|
| Ag | −0.175 | 6.209 |
| Ag/CeM/GNS-5 | −0.148 | 0.388 |

Figure 9(b) shows electrochemical impedance spectra of Ag and Ag/CeM/GNS-5 in 3.5 wt.% NaCl solution, which are fitted by equivalent circuit. The fitting results are shown in Table 3, where $R_s$ is the solution resistance between the sample and the reference electrode; $R_{ct}$ is the charge transfer resistance; $R_c$ is the resistance of the coating; $Q_c$ is the capacitance; $Q_{dl}$ is the double-layer capacitor, which reflects the impedance of the sample [28]. The $R_{ct}$ values of Ag and Ag/CeM/GNS-5 were 92.21 and 4592 Ω·cm$^2$, respectively. Therefore, the corrosion resistance of Ag/CeM/GNS-5 was much better than that of Ag coating, indicating that superhydrophobic surface could greatly improve the corrosion resistance of Ag coating.

Superhydrophobic surface has a rough micro-nano structure, which can store air and form an air film. Figure 10 shows the corrosion protection mechanism of Ag/CeM/GNS composite coating in corrosive medium. When the silver coating is placed in a corrosive medium, the ions and water in the solution directly contact the surface of the silver layer and begin to corrode its surface. If the Ag/CeM/GNS composite coating is placed in

**Table 3** Impendence fitting results of Ag and Ag/CeM/GNS-5 in 3.5 wt.% NaCl solution

| Coating | $R_s$/(Ω·cm$^2$) | $Q_c$/(F·cm$^2$) | $R_c$/(Ω·cm$^2$) | $Q_{dl}$/(F·cm$^2$) | $R_{ct}$/(Ω·cm$^2$) |
|---|---|---|---|---|---|
| Ag | 9.889 | $1.182\times10^{-4}$ | 32.9 | $1.304\times10^{-2}$ | 92.21 |
| Ag/CeM/GNS-5 | 187.3 | $1.327\times10^{-5}$ | 1206 | $1.965\times10^{-4}$ | 4592 |

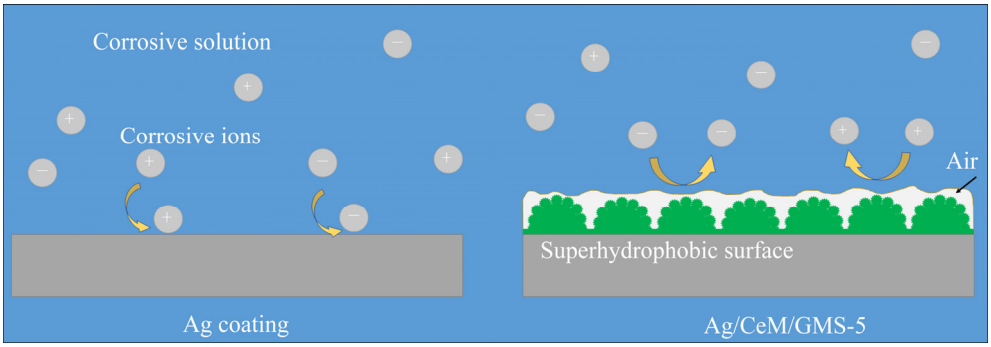


**Fig. 10** Anti-corrosion mechanism of Ag/CeM/GNS composite coatings in corrosive medium

corrosive medium, due to its superhydrophobic surface, the air layer formed on the surface can separate the coating from the corrosive solution. This is the internal mechanism of corrosion resistance of Ag/CeM/GNS composite coating.

## 4 Conclusions

(1) Silver coating was prepared on TPU surfaces via two-component spraying method, then the superhydrophobic surface was obtained by one-step electrodeposition. The CA of as-prepared Ag/CeM/GNS composite coatings could reach as high as 154.1°, while SA was as low as 1°.

(2) The obtained Ag/CeM/GNS composite coating possesses a low resistivity of 0.494 Ω·mm, which decreased by 27.2% compared with that of Ag coating.

(3) The Ag/CeM/GNS composite coatings could conduct the circuit normally in the states of tension, bending and twisting deformation, showing excellent mechanical stability and applicability.

(4) The as-prepared Ag/CeM/GNS composite coatings showed excellent self-cleaning and anti-fouling properties, and the corrosion resistance of Ag/CeM/GNS composite coatings in 3.5 wt.% NaCl solution was improved significantly compared with that of original Ag coating.

## Acknowledgments

The authors gratefully acknowledge financial support from the National Natural Science Foundation of China (No. 52105186), the Guangdong Basic and Applied Basic Research Foundation, China (Nos. 2019A1515011282, 2022A1515011547, 2021B1515120014), and the Fangchenggang Scientific Research and Technology Development Project, China (No. AB21014008).

## References

[1] LI Dong-dong, LAI Wen-yong, ZHANG Yi-zhou, HUANG Wei. Printable transparent conductive films for flexible electronics [J]. Advanced Materials, 2018, 30: 1704738.

[2] ZHANG Dong-lan, WANG Jiong, KONG Yi, ZOU You, DU Yong. First-principles investigation on stability and electronic structure of Sc-doped $\theta'$/Al interface in Al−Cu alloys [J]. Transactions of Nonferrous Metals Society of China, 2021, 31: 3342−3355.

[3] LIU Xing, LI Dong-dong, CHEN Xin, LAI Wen-yong, HUANG Wei. Highly transparent and flexible all-solid-state supercapacitors based on ultralong silver nanowire conductive networks [J]. ACS Applied Materials & Interfaces, 2018, 10: 32536−32542.

[4] TEE C K B, OUYANG J Y. Soft electronically functional polymeric composite materials for a flexible and stretchable digital future [J]. Advanced Materials, 2018, 30: e1802560.

[5] ZHOU Lu, YU Meng-jie, CHEN Xiao-lian, NIE Shu-hong, LAI Wen-yong, SU Wen-ming, CUI Zheng, HUANG Wei. Screen-printed poly(3,4-ethylenedioxythiophene): Poly (styrenesulfonate) grids as ITO-free anodes for flexible organic light-emitting diodes [J]. Advanced Functional Materials, 2018, 28: 1705955.

[6] MEI Xiao-kang, LU Long-sheng, XIE Ying-xi, WANG Wen-tao, TANG Yong, TEH K S. An ultra-thin carbon-fabric/graphene/poly(vinylidene fluoride) film for enhanced electromagnetic interference shielding [J]. Nanoscale, 2019,

11: 13587−13599.

[7] LI Dong-dong, LAI Wen-yong, FENG Fang, HUANG Wei. Post-treatment of screen-printed silver nanowire networks for highly conductive flexible transparent films [J]. Advanced Materials Interfaces, 2021, 8: 2100548.

[8] DING Ya-ru, XUE Chao-hua, GUO Xiao-jing, WANG Xue, JIA Shun-tian, AN Qiu-feng. Fabrication of TPE/CNTs film at air/water interface for flexible and superhydrophobic wearable sensors [J]. Chemical Engineering Journal, 2021, 409: 128199.

[9] QIU Hui-jing, SONG Wei-zhi, WANG Xiao-xiong, ZHANG Jun, FAN Zhi-yong, YU Miao, RAMAKRISHNA S, LONG Yun-ze. A calibration-free self-powered sensor for vital sign monitoring and finger tap communication based on wearable triboelectric nanogenerator [J]. Nano Energy, 2019, 58: 536−542.

[10] SHI Xiang, ZUO Yong, ZHAI Peng, SHEN Jia-hao, YANG Yi-wei, GAO Zhen, LIAO Meng, WU Jing-xia, WANG Jia-wei, XU Xiao-jie, TONG Qi, ZHANG Bo, WANG Bing-jie, SUN Xue-mei, ZHANG Li-hua, PEI Qi-bing, JIN Da-yong, CHEN Pei-ning, PENG Hui-sheng. Large-area display textiles integrated with functional systems [J]. Nature, 2021, 591: 240−245.

[11] MA Wei-ting, LI Xin-yi, LU Hong-bo, ZHANG Mao-qin, YANG Xiao-fei, ZHANG Ting-ting, WU Li-feng, CAO Guo-zhong, SONG Wei-xing. A flexible self-charged power panel for harvesting and storing solar and mechanical energy [J]. Nano Energy, 2019, 65: 104082.

[12] ZENG Jing, PENG Chao-qun, WANG Ri-chu, LIU Ya-jing, WANG Xiao-feng, LIU Jun. Preparation of dual-shell Si/$TiO_2$/CFs composite and its lithium storage performance [J]. Transactions of Nonferrous Metals Society of China, 2019, 29: 2384−2391.

[13] HE Ye-qing, KANG Zhi-xin, CHEN De-xin. Integrating nanodiamonds to improve anticorrosion property and conductivity simultaneously of Ag composite films via layer by layer spin-spray deposition [J]. Applied Surface Science, 2020, 505: 144643.

[14] LU Wei, XU Yun, ZOU Yu-xiao, ZHANG Lin-ao, ZHANG Jiu-shuang, WU Wei-tong, SONG Guo-feng. Corrosion-resistant and high-performance crumpled-platinum-based triboelectric nanogenerator for self-powered motion sensing [J]. Nano Energy, 2020, 69: 104430.

[15] WANG Zhi-hu, ZHANG Ju-mei, LI Yan, BAI Li-jing, ZHANG Guo-jun. Enhanced corrosion resistance of micro-arc oxidation coated magnesium alloy by superhydrophobic Mg/Al layered double hydroxide coating [J]. Transactions of Nonferrous Metals Society of China, 2019, 29: 2066−2077.

[16] LIU Qin, CHEN De-xin, KANG Zhi-xin. One-step electrodeposition process to fabricate corrosion-resistant superhydrophobic surface on magnesium alloy [J]. ACS Applied Materials & Interfaces, 2015, 7: 1859−1867.

[17] WU Li-sheng, WANG Ling, GOU Zheng, LUO Jun-chen, XUE Huai-guo, GAO Jie-feng. Durable and multifunctional superhydrophobic coatings with excellent joule heating and electromagnetic interference shielding performance for flexible sensing electronics [J]. ACS Applied Materials & Interfaces, 2019, 11: 34338−34347.

[18] KANG Zhi-xin, ZHANG Yang, ZHOU Ming-qiang. AgNPs@CNTs/Ag hybrid films on thiolated PET substrate for flexible electronics [J]. Chemical Engineering Journal, 2019, 368: 223−234.

[19] ZENG Xiao-yan, ZHANG Qi-kai, YU Rong-min, LU Can-zhong. A new transparent conductor: Silver nanowire film buried at the surface of a transparent polymer [J]. Advanced Materials, 2010, 22: 4484−4488.

[20] NOVOSELOV K S, FAL′KO V I, COLOMBO L, GELLERT P R, SCHWAB M G, KIM K. A roadmap for graphene [J]. Nature, 2012, 490: 192−200.

[21] DEEPI A S, NESARAJ A S. Design of best performing hexagonal shaped Ag@CoS/rGO nanocomposite electrode material for electrochemical supercapacitor application [J]. Transactions of Nonferrous Metals Society of China, 2020, 30: 2764−2774.

[22] ZHOU Ming-qiang, KANG Zhi-xin, ZHU Shi-meng. Preparation of Ag/graphene composite films by three-component spray-spin-spray coating on surface modified PET substrate [J]. Nanotechnology, 2019, 30: 395701.

[23] WU Ying, WANG Zhen-yu, LIU Xu, SHEN Xi, ZHENG Qing-bin, XUE Quan, KIM J K. Ultralight graphene foam/conductive polymer composites for exceptional electromagnetic interference shielding [J]. ACS Applied Materials & Interfaces, 2017, 9: 9059−9069.

[24] AYYAPPAN S, GOPALAN R S, SUBBANNA G N, RAO C N R. Nanoparticles of Ag, Au, Pd, and Cu produced by alcohol reduction of the salts [J]. Journal of Materials Research, 1997, 12: 398−401.

[25] DHAKAL R, JUNG Y, PARK H, CHO G, KIM N Y. Screen-printed flexible bandstop filter on polyethylene terephthalate substrate based on Ag nanoparticles [J]. Journal of Nanomaterials, 2015, 2015: 1−8.

[26] NGUYEN V H, KIM B K, JO Y L, SHIM J J. Preparation and antibacterial activity of silver nanoparticles-decorated graphene composites [J]. The Journal of Supercritical Fluids, 2012, 72: 28−35.

[27] ZHANG Jun-yi, KANG Zhi-xin. Effect of different liquid-solid contact models on the corrosion resistance of superhydrophobic magnesium surfaces [J]. Corrosion Science, 2014, 87: 452−459.

[28] ZHOU Y H, XIE F Q, WU X Q, ZHAO W D, CHEN X. A novel plating apparatus for electrodeposition of Ni−SiC composite coatings using circulating-solution co-deposition technique [J]. Journal of Alloys and Compounds, 2017, 699: 366−377.

# 一步电沉积制备稳定性优异的强健超疏水 Ag/石墨烯涂层

陈德馨[1,2]，何叶青[3]，王启伟[1]，李 卫[1]，康志新[3]

1. 暨南大学 先进耐磨蚀及功能材料研究院，广州 510632；
2. 暨南大学 韶关研究院，韶关 512027；
3. 华南理工大学 机械与汽车工程学院，广州 510640

**摘 要**：提出一种用于柔性电子器件可拉伸银基复合涂层的制备方法，该涂层具有优导的导电性和稳定性。首先采用双组分喷涂法在弹性基板热塑性聚氨酯(TPU)弹性体橡胶表面制备银涂层，通过一步电沉积铈化合物(CeM)和石墨烯纳米片(GNS)获得超疏水表面，即 Ag/CeM/GNS 复合涂层。经多次弯曲和拉伸，Ag/CeM/GNS 复合镀层仍具有较高的电导率，且复合涂层具有良好的自清洁和防污性能，耐腐蚀性较原 Ag 涂层显著提高。此外，Ag/CeM/GNS 复合涂层在拉伸、弯曲和扭转等变形状态下仍正常导电，具有良好的力学稳定性和适用性。因此，所研制的 Ag/CeM/GNS 复合镀层具有优良的导电性能和稳定性，在苛刻条件下服役的柔性电子器件中具有广阔的应用前景。

**关键词**：银/石墨烯涂层；超疏水性；一步电沉积；稳定性

**(Edited by Wei-ping CHEN)**